Project Final Report
Award #DE-SC-0001992
(submitted September 20, 2013)

"Assessment of Proton Deflectometry for Exploding Wire Experiments"

Principle Investigator (PI): **Prof. Farhat Beg (UCSD)**
Co-PI: **Dr. Mingsheng Wei (UCSD)**

Executive Summary

Proton radiography has been widely used as a method of assessing the magnitude and structure of electromagnetic fields generated in laser-plasma interaction experiments. It has proven to be a valuable tool for verifying theory, validating code, and providing general insight into the dynamics of high-energy-density physics systems. Its implementation for laser experiments was a natural evolution, since multiple laser beams are often available within a single target chamber. For this reason, proton deflectometry has primarily been used in such facilities, where additional beams may be used to readily produce high energy protons for use as a diagnostic tool. Few z-pinch facilities are equipped with short-pulse high-intensity lasers capable of producing diagnostic protons. In the U.S., only two such facilities are in place, namely the Z-Petawatt high intensity laser & Z-R at Sandia National Laboratories, and the Leopard laser & Zebra at the Nevada Terawatt Facility. The implementation of this technique in pulsed-power-produced plasma experiments is crucial to verifying theory and answering long-standing questions about electromagnetic field topology of the system. Measurements of the field topology through other means have proven unreliable and limited in scope. For example, electrical probes have been used to this end, but are subject to mega-volt potentials, which often cause failure early in the experiment. There is also the question of charge-screening interference with such probes. Optical Faraday rotation has also been applied, but is limited to areas where the density of the plasma is below the critical density to allow propagation through the system and free of strong gradients.

This project provides the first demonstration of the application of proton deflectometry for the diagnosis of electromagnetic field topology and current-carrying regions in Z-pinch plasma experiments. Over the course of this project several milestones were achieved. High-energy proton beam generation was demonstrated on the short-pulse high-intensity Leopard laser, (10 Joules in ~350 femtoseconds, and the proton beam generation was shown to be reproducible. Next, protons were used to probe the electromagnetic field structure of short circuit loads in order to benchmark the two numerical codes, the resistive-magnetohydrodynamics (MHD) code, Gorgon, and the hybrid particle-in-cell code, LSP for the interpretation of results. Lastly, the proton deflectometry technique was used to map the magnetic field structure of pulsed-power-driven plasma loads including wires and supersonic jets formed with metallic foils. Good agreement between the modeling and experiments has been obtained. The demonstrated technique holds great promise to significantly improve the understanding of current flow and electromagnetic field topology in pulsed power driven high energy density plasmas. Proton probing with a high intensity laser was for the *first time* implemented in the presence of the harsh debris and x-ray producing z-pinch environment driven by a mega-ampere-scale pulsed-power machine.

The **intellectual merit** of the program was that it investigated strongly driven MHD systems and the influence of magnetic field topology on plasma evolution in pulsed power driven plasmas. The experimental program involved intense field-matter interaction in the generation of the proton probe, as well as the generation of plasma subjected to 1 MegaGauss scale magnetic fields. The computational aspect included two well-documented codes, in combination for the *first time* to provide accurate interpretation of the experimental results. The **broader impact** included the support of 2 graduate students, one at UCSD and one at NTF, who were exposed to both the experimental physics work, the MHD and PIC modeling of the system. A first generation college undergraduate student was employed to assist in experiments and data analysis throughout the project. Data resulting from the research program were broadly disseminated by publication in scientific journals, and presentation at international and national conferences and workshops.

1. Introduction

Proton radiography has been widely used as a method of assessing the magnitude and structure of electromagnetic fields generated in laser-plasma interaction experiments. It has proven to be a valuable tool for verifying theory, validating code, and providing general insight into the dynamics of high-energy-density physics systems [1-6]. Its implementation for laser experiments was a natural evolution, since multiple laser beams are often available within a single target chamber. For this reason, proton deflectometry has primarily been used in such facilities, where additional beams may be used to readily produce high energy protons for use as a diagnostic. Few z-pinch facilities are equipped with short-pulse high-intensity lasers capable of producing diagnostic protons. In the U.S., only two such facilities are in place, namely the Z-Petawatt high intensity laser & Z-R at Sandia National Laboratory, and the Leopard laser & Zebra at the Nevada Terawatt Facility. The implementation of this technique in pulsed-power-produced plasma experiments is crucial to verifying theory and answering long-standing questions about electromagnetic field topology of the system

Novel methods to determine the current flow position or magnetic field topology are necessary due to the difficulty in making accurate measurements of exploding wire experiments. The high voltage at which MA scale generators operate (typically 1-2 MV) combined with high field gradients cause electrical probes to breakdown at some point during an experiment, and so measurements are useful only for a limited period of time. The possibility of charge screening also raises further issues. For these reasons a non-invasive method for determining of the B-field structure is highly desirable. In addition, whilst data recovered using methods such as electric probes is extremely valuable during the period in which the signal is deemed reliable, the B-field variation is only recovered at one spatial location for each probe. This can be improved by placing probes at multiple positions during a single experiment, but eventually these probes will cause too large of a perturbation of the system.

Therefore a method which provides both temporal and spatial resolution of the magnetic field structure would be ideal. This can be achieved using multiple frame imaging techniques. One such method which has been applied successfully to a variety of plasma environments is Faraday rotation. The orientation of a plane polarized laser beam is rotated by interaction with a plasma in a magnetic field, to an extent determined by the line integral of the field strength and the electron density along the probe path. To deconvolve the field strength at a location therefore requires knowledge of the electron density at the same moment as the degree of rotation of the laser beam. This method can therefore only be applied to well-characterized systems or must rely on uncertain assumptions.

Spectroscopic techniques such as Zeeman splitting have also been applied in some related plasma systems. In exploding wire experiments, and especially in wire arrays, the recovery of B-field strength is often complicated by the local plasma parameters. Temperatures range from a few eV to several keV providing a large thermal broadening which may mask the Zeeman component, and the plasma system may be expanding or imploding providing an additional Doppler shift to the spectroscopic signature. In addition, these parameters may vary rapidly as a function of space and time. These factors therefore necessitate the recovery of the entire plasma parameter range with both spatial and temporal resolution, before an assessment of the Zeeman effect can be deduced. This is difficult if not impossible to achieve, even in the most advanced of experimental set-ups.

A diagnostic method which has significant potential to aid in all the situations discussed above is Proton Probing, described in this section. The use of protons as a probe for matter has opened a large and exciting range of research areas and applications. The new generation of short pulse laser-driven proton beams is at the scientific cutting edge of relativistic laser-matter interactions with laser intensities greater than 10^{18} Wcm^{-2}. The observation of a highly collimated intense proton beam was first seen by Key *et al* [7] on the Nova laser at Lawrence Livermore National Laboratory. At the same time, a similar finding was made by the Imperial College group on the Vulcan 100 TW facility at Rutherford Appleton Laboratory [8]. In these experiments, a highly collimated proton beam was observed to emit from the back side of a thin foil target with its front surface irradiated by a high intensity (>10^{19} Wcm^{-2}) short pulse (~ps) laser. These protons mainly originate from natural impurity layers of water vapor and hydrocarbons on the target surface.

The proton beams produced under such conditions were bright, typically containing more than 10^{12} protons with energies greater than 3 MeV and having broad energy spectrum. Due to its extremely small source size, low emittance, and short pulse duration, a time resolving point projection probe scheme can be easily obtained. Because of these unique properties, such beams were proposed as an important diagnostic method for probing plasmas, as it is sensitive to both density and electromagnetic fields.

2. Project Milestones and Achievements:

a) Proton Beam Generation

The first step in the implementation of proton deflectometry for z-pinch experiments was to characterize the proton beams that could be produced by the Leopard laser at the Nevada Terawatt Facility (NTF). The Leopard short pulse laser (1053 nm wavelength) consistently delivered up to 12 J energy in ~350 fs pulse duration, which was focused to a ~7.5 μm diameter spot at normal incidence, giving an on-target peak laser intensity > 10^{19} W cm^{-2}. At such intensities, the Target Normal Sheath Acceleration (TNSA) mechanism

generated the protons for use as probing particles [9]. In this regime, fast electrons are generated by a relativistic laser matter interaction at the front (laser-facing) side of the target. These fast electrons then exit the rear surface of the target, setting up a strong electric field. This electric field is responsible for the subsequent acceleration of protons from the rear surface. Proton beam generation and optimization were performed first off-line in the Phoenix target chamber, where the optical table was decoupled from the vacuum chamber, minimizing any motions associated with evacuation of the chamber, which may adversely affect the focus of the laser beam on target and thus degrade proton production. In order to produce the highest energy proton beam possible with the given laser specifications, extensive parameter space was examined. Various target thicknesses, ranging from 2-50 μm, and materials, Au, Cu, and Ti were tested as candidates. Ultimately, the experimenters determined that the optimal targets were 1.5 x 1.5 mm, 2 μm thick Titanium foils glued to thin glass support-stalks. To enable use of such thin targets, the Leopard power contrast, the ratio of the power in the pre-pulse, or Amplified Spontaneous Emission, to the power in the main pulse, was required to be at most 10^{-7}. This was achieved after a recent upgrade to the Leopard laser, namely the inclusion of two new fast Pockels cells, which enabled the preferential selection of the main laser pulse over the ASE. The primary diagnostic used for the detection of the proton beam was radiochromic dosimetry film, or RCF. RCF has been extensively used for this purpose in the past for laser-accelerated proton beam experiments. This detector was chosen for several reasons, some of which will be discussed in the following section.

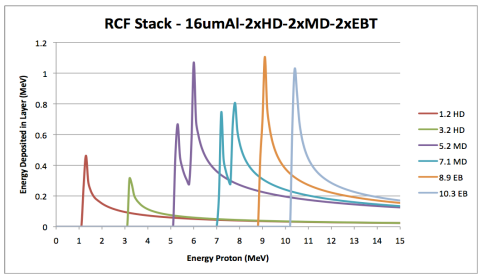

Fig 1. Projected proton energy deposited in each layer of a specific RCF detector stack. The stack is comprised of 2 layers of Gafchromic® HD-810, MD, and EBT respectively wrapped in 16µm Al foil.

The proton energy spectrum was directly proportional to the average hot electron energy, which was approximately proportional to a Boltzmann exponential [10]. Protons with a maximum energy > 10 MeV were observed with the given parameters. There was a distinct advantage using a proton probe with a broad energy spectrum, as opposed to a mono-energetic proton source, as in other proton deflectometry experiments that utilized mono-energetic protons [11-14]. Combining with the multiple layers of RCF as proton beam detectors in tandem with various combinations of films and filter materials, different energies within the proton spectrum were able to be resolved. A Bragg peak absorption in each layer ensured that the majority of signal detected on each RCF layer was within a well-defined energy band. This energy band was determined via a dE/dx calculation, which utilized the SRIM code [14]. The calculated response for a typical RCF film stack configuration is shown in Fig 1. This configuration was fielded for the experimental results shown in Fig. 2, which displays a sample proton spectrum produced by Leopard. The RCF detector stack was located 25 mm behind the target, and was completely wrapped in light-tight 16 μm thick Al to reduce signals from other high-energy sources (e.g. <5 keV photons, electrons <7 MeV, ions of carbon, oxygen and titanium). Low energy protons deposit their energy within the front layers of the film

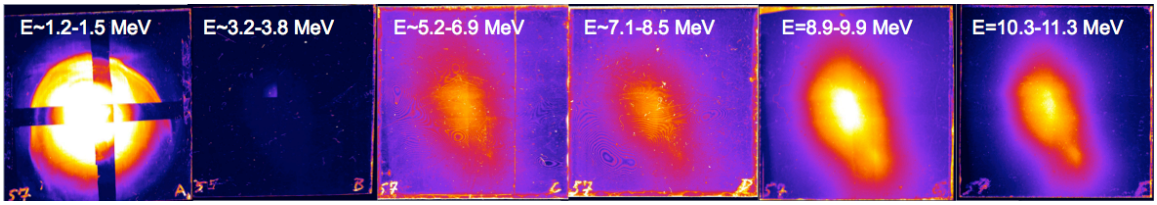

Fig 2. Signal on RCF film stack. Different film types used in the detector pack increased in sensitivity every two layers (layers 3-4 are ~100x more sensitive than 1-2, and 5-6 are ~100x more sensitive than 3-4) in order to detect the higher-energy, lower-flux component of proton beam. Two 16 μm thick, 3 mm wide, Al foil strips crossed the film pack to assess ability of low-energy component of proton beam to permeate 16, 32, and 48 μm of Al.

stack, and higher energy protons deposit their energy deeper within the film stack. Since the different energies correspond to different velocities, this means that different temporal snapshots of the same system can be taken during a single shot. For a typical system size of ~ 40 mm, and an energy spread and detector setup as in Fig. 1, the temporal difference between the first and last layer of film was ~2 ns. For example, a 1.2 MeV proton will take ~ 2.6 ns whereas a 10 MeV proton will take ~0.9 ns. Since a typical Z-pinch experiment occurs over the course of 50 ns to 1 μs, this provides excellent temporal resolution of magnetic field and current measurements. Therefore, the advantage of using multiple RCF layers in these experiments is that each layer provides data from protons of a distinct energy, allowing multiple measurements for benchmarking.

b) **Proton Deflectometry Experiments and Code Benchmarking**

Once the proton source was well-characterized, the next step was to test the technique on short-circuit loads. Short circuit loads were the ideal candidates primarily for three reasons. One reason was that for appropriately chosen rod diameters, little or no x-ray background was created, which could have ablated the side of the proton target facing the load, which would potentially interfere with the production and detection of the proton beam. Secondly, there was no debris launched from the load, which could have severely damaged the RCF detectors. Lastly, they produced uniform electromagnetic fields, which were simple to analyze and model. Combining these three advantages over plasma loads, it was reasoned that the data collected from these tests would be prime data for benchmarking the codes, Gorgon [15] and LSP [16], used in this project. Benchmarking the codes was of paramount importance before applying proton deflectometry to plasma loads, which can have far more complicated electromagnetic geometries. More details concerning the simulations are presented later in the report.

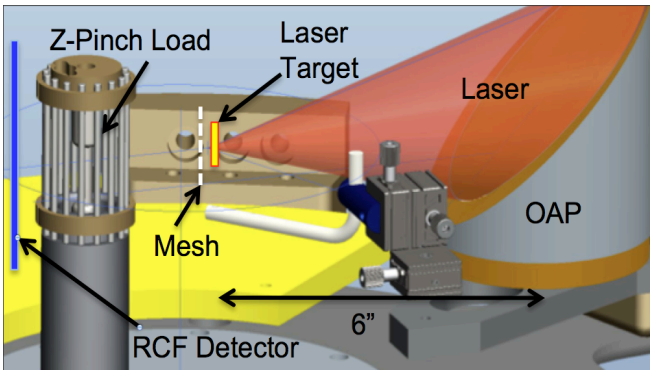

Fig. 3. Schematic of the experimental set up for proton deflectometry of short circuits.

The experimental geometry is shown in Fig. 3. A proton beam was produced by the short-pulse high-intensity laser solid target interaction, and directed in the radial direction with respect to the z-axis of a short circuit load driven by Zebra, which is capable of delivering 1.6 MA peak current with a 100 ns, 0-100% current rise time. In these experiments it was operated in long pulse mode, delivering 0.6 MA peak current with a 200 ns, 0-100% rise time. The initial field measurements were done with short-circuit loads comprised of either 6 mm or 3 mm diameter stainless steel rods, giving calculated peak fields at the surface of the conductor of 40 T and 80 T respectively. This allowed for not only a slightly less hostile environment in terms of the vibrations experienced by the laser beam transport and optics within the Zebra chamber, but also allowed for a slower variation in the fields, making the quasi-static magnetic fields approximation more valid. For quantification of proton beam distortions due to the observed magnetic field, a thin ~20 μm thick copper mesh was placed in the path of the proton beam, near the laser target. The copper mesh was then imprinted on the beam, so that distortions were more apparent, and more easily compared to simulations of the experiment.

In the first layer of film (as shown in Fig. 4), the contrast of the grid was very good, however, the contrast was severely degraded as the proton beam energy is increased, e.g. the film layer depth increased. This is in agreement with predictions made based on NIST PSTAR stopping ranges, which predicted the maximum path length of 1.25 MeV protons, typically the minimum detected proton energy in these experiments, to be < 10 μm in solid Cu, whereas 5 MeV protons had a range of > 75 μm. An example of this observation is seen in Fig. 4, where a proton beam is detected at a distance of 55 mm from the proton target, after it has passed through the Zebra short circuit hardware, while no current was present in the system, and thus no deflection occurred. Typically, the distance between the grid and the target varied from 1-2 mm, so the magnification of the grids on the film varied between ~27-56, and occasionally was slightly rotated relative to the target plane, and thus produced an image like the one shown in Fig. 4, where the magnification is different across the image. The large dark features on the images are shadows of the short circuit hardware, including the 6 mm diameter central conductor, and several of the 3 mm diameter return-current posts. The nearly horizontal line across the center is a 400 μm Cu wire, which was placed directly in front of the detector pack as a fiducial.

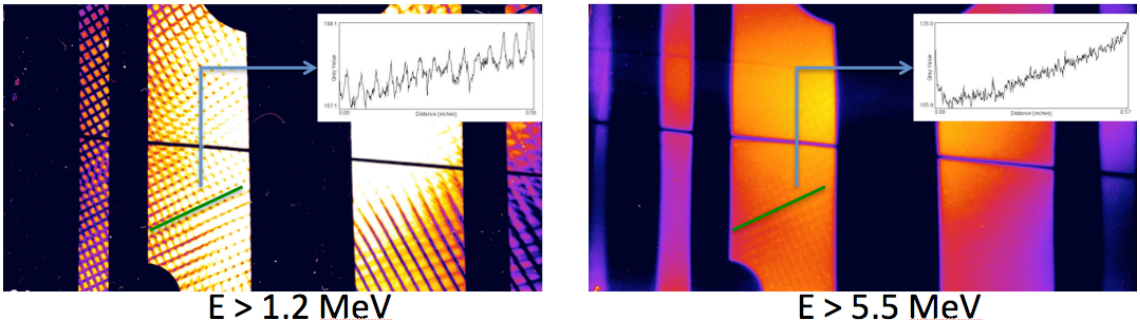

Fig. 4. Two layers of RCF from the same shot are compared. Grid contrast was degraded significantly when proton energy reached 5 MeV, as demonstrated by the grid profile plots taken along the grid at the same location for both images. Good contrast remained for the 400 μm diameter Cu wire through all observed energies.

Next, coupled Leopard and Zebra shots gave the first field measurements via proton deflectometry. The setup given above remained the same for the coupled shots, except that the film sizes were increased in order to capture the desired features. The size increase was deemed necessary from initial predictions made by the simulation work completed prior to the experimental series. For the experimental geometry used, protons were deflected away from the short circuit in the outward-radial direction. During the course of the deflection, protons also experienced an axial displacement (Fig. 5). Combining the two displacements, a radially and vertically offset deflection pattern was observed.

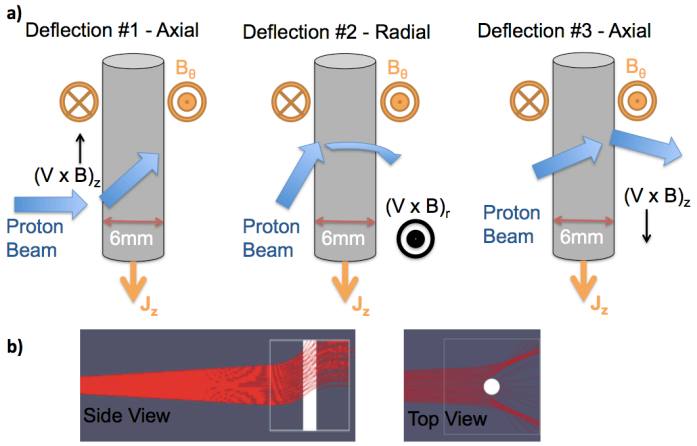

Fig. 5: (a) Schematic of three-stage deflection experienced by a protons passing near short circuit magnetic fields. (b) Two views of particle deflection trajectories from Gorgon illustrating stages of deflection.

The inherent divergence of the proton beam leads to a feature in the data that provides information about the magnetic field strength. The divergence means that different regions of the beam were affected differently, with the initially upward travelling protons experiencing a larger initial deflection, which then contributed to a larger radial deflection than those with an initially downward trajectory. This translated to a characteristic angle between the deflection features, which is largely independent of the exact divergence angle of the proton beam, but was highly dependent on the magnitude of the azimuthal magnetic field. This effect is displayed in Fig. 6, where results from a 6 mm short circuit field carrying 565 kA current produced a maximum surface field of 37.6 T which split the initially round probing beam into two symmetrically diverging features. At the outer edges of the deflection features, the shadows of two outer return-current posts can be seen. As the current in the load was increased, or the diameter was reduced, the magnitude of the magnetic field at the surface of the conductor was increased, and a larger angle between the deflection features was observed as expected. This effect was reproduced in both Gorgon and LSP simulations. Over the divergence angle range explored in simulations, typically between 45 to 90 degrees full angle, the divergence angle of the beam merely determined the vertical extent of the deflection feature, while the angle between the deflection features was nearly constant for the given field strength. It is worth noting that when a proton beam with no divergence was used, there was no angle between the two deflection features, though they were still spatially separated in the horizontal direction. Fortunately, the true divergence angle of the laser produced proton beams in this experiment lie within the 45-

90 degree range, where the field measurement is the most important factor in determining the angle between the features. In Fig. 6b, a change in angle is observed between the

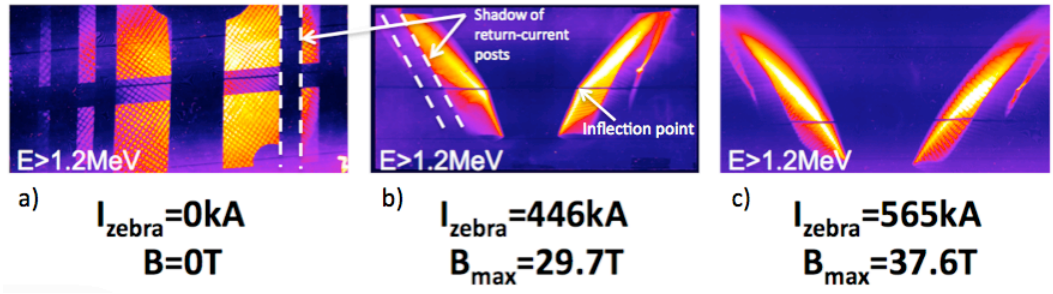

Fig. 6: (a) a proton beam with a mesh imprinted is sent through the short circuit load hardware with no Zebra current flowing. (b,c) Distorted proton beam with a mesh imprinted is deflected radially away from the vertical short circuit for two different current and magnetic conditions.

upper and lower half of the beam, since a portion of the proton beam has collided with the central conductor, thereby truncating the beam at a minimum diameter and creating an apparent inflection point in the beam.

In order to interpret the results of the proton deflectometry experiments and obtain magnetic field information quantitatively, a numerical simulation capability was necessitated. Two codes were used to simulate the deflectometry result, and were subsequently benchmarked at the same time with the data collected. Two codes used in this project were the 3D resistive MHD code, Gorgon, and the hybrid particle-in-cell code LSP (Large Scale Plasma). Here Gorgon was used to simulate the current flow and the field generation by the short-circuit load, including the details of the load hardware used in the experiment. Gorgon has recently incorporated a proton-probing post-processor, which calculated the integrated proton paths from the source, through the magnetic field generated by the load, and finally on to a detector. Fig 7 shows the comparison of the measured RCF deflection and the Gorgon simulated deflection results. Gorgon and LSP simulations reproduced the data quite well, with reasonable agreement between separations and angles in the features.

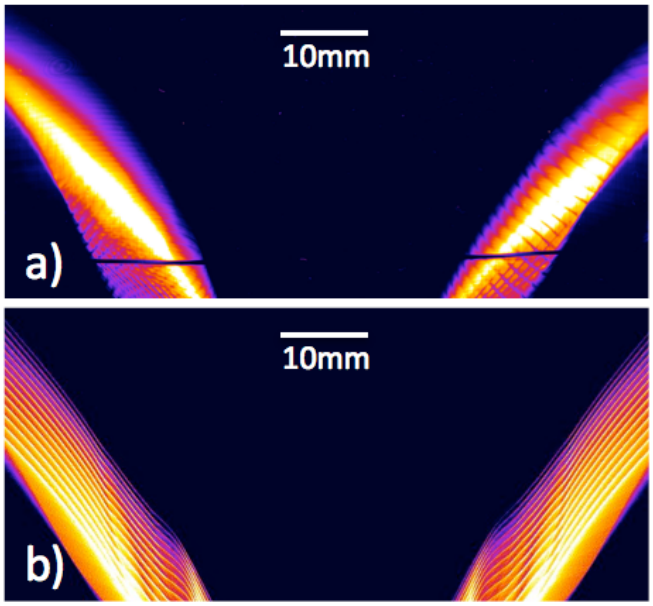

Fig. 7. a) Experimental RCF detection of deflected proton beam at t=+30 ns after peak Zebra current, I=565 kA. b) Gorgon proton-probing simulation at same time. Signal scales for both are in arbitrary units, and d=6 mm for the short circuit load.

It should be noted that the post-processor particle tracking method included in the Gorgon code is subject to several limitations as it is limited to mono-energetic proton beams with uniform spatial distribution, and does not include any collisional effects, such as those from encounters with load hardware, or plasma-proton beam interactions. Due to these limitations, the other code, LSP, is necessary to take these factors into account, and thus a more complete representation of the experiment is produced. Using the same short circuit magnetic field data from the Gorgon modeling as initial conditions for both codes, the two codes were benchmarked against each other. In order to simulate the deflected proton trajectories in LSP, the load is first simulated using Gorgon. The Gorgon output of magnetic field and plasma density is then translated to the 3D LSP simulation grid as initial conditions, and these parameters are held static throughout the simulation in both Gorgon particle tracking post-processing and the LSP modeling. This is a reasonable approximation, since the proton beam traverses the field region in ~1 ns, and the z-pinch evolves over the course of ~200 ns. A proton beam is then injected with characteristics similar to those observed in the experiment, e.g. energy and divergence, and tracked as it traverses the field region. The final beam pattern is then collected on a detector of similar size and location as in the experiment.

An example of the proton tracking in LSP is shown in Fig. 8, and a similar example of tracing in Gorgon is shown in Fig. 5b. Several small differences were present in the comparison of the experiment and simulations, however, they did not invalidate the predictions. The mesh imprint on the beam was not present

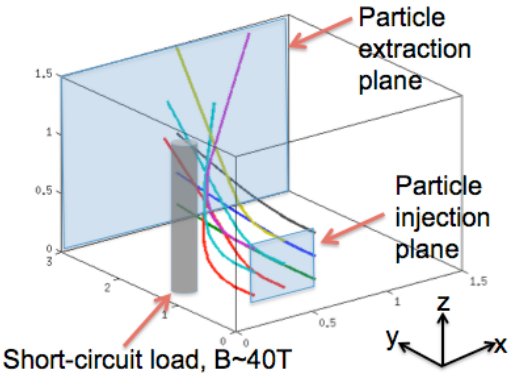

Fig. 8. Traces of test-particle proton trajectories while passing near a 6mm diameter short circuit conductor carrying a 600kA current. Particle injection and extraction planes are shown for reference. Spatial units are in centimeters.

in these Gorgon simulations, nor was the stopping due to the return-current posts, although the latter is visible as a vertical distortion in the simulated proton beam in Fig. 6. Another reason for the slight variation in the results between experiment and simulation is that the beam profile generated by Gorgon is square, rather than circular, which makes very little difference in the final result. Simulations with LSP were shown to produce the same results, though at a significantly higher computational cost, leading to the increased reliance on Gorgon's post-processor for the calculations. LSP calculations were primarily reserved for the exploration of interaction phenomena to assess the importance of these factors in the calculations. It was found that in general, the inclusion of such physics had little or no effect on the final outcome. The only significant effects appeared where they were to be expected, in the lowest energy components of the proton beam < 3 MeV. In this regime, proton collisions with the plasma led to an overall reduced signal on the RCF. It was found that these effects could be accounted for by using density profiles from the simulations in tandem with SRIM calculations to determine the lower limit of proton energy for each region.

Applying the proton probing method to plasma systems presented several challenges. For many loads, significant XUV and x-ray emission may generated, which have the potential to initiate ablation on the laser target. If there is significant plasma generated on the rear surface of the proton foil target, the sheath field necessary for accelerating protons may be adversely affected. The radiation from the load could also potentially generate enough of a background signal on the RCF to make it difficult to identify the proton signal. For the first tests with Z-pinch plasma loads, a radial foil load was chosen. Compared to many other load choices, this was an ideal candidate to aid in overcoming the previously mentioned challenges. The primary benefit of using such a system was that the debris were mostly directed in the vertical direction, keeping the RCF detector and the OAP clear of damage.

Like most z-pinch systems, the general dynamics of these systems can be

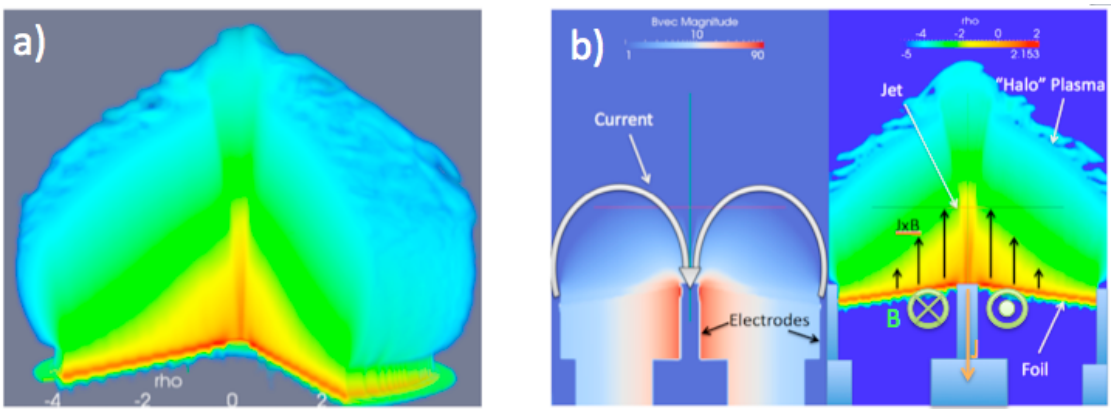

Fig. 9. Gorgon simulations showing (a) 3D view of plasma mass density at 300 ns after Zebra current start, or 100 ns after peak current, with a portion cut away. (b) RZ-plane slice through magnetic field and mass density at same time. Magnetic field slice outlines where current carrying region has moved since initially being confined near the surface of the foil, and orientation of magnetic field. Mass density slice shows details of radial foil system including the jet and the "halo".

qualitatively illustrated with an examination of the JxB force present in the system. Figure 9(b) displays a schematic of this behavior for a radial foil load. A 12.5 um Al foil is stretched across the electrodes, while the cathode contacts the bottom surface. The experimental layout is shown in Figure 10(a). Current flows radially through the foil and down through the cathode, where a large magnetic field is created around the electrode just below the surface. This directs the JxB force in the upward z-direction. The foil begins to ablate, and the rate of mass ablation is proportional to the current density, which increases as the radius decreases, creating a gradient in the density above the foil. Just above the electrode, little/no current flows, so no ablation occurs here. This creates a void in the ablated plasma distribution above the foil, which in turn sets up a density gradient which is responsible for the acceleration of a collimated jet in the center of this "halo" plasma. As more plasma is ablated, the region where current is initially confined to flow begins to move further away. The path further away from the foil was of lower inductance, and current flows near the surface of the halo, and back down through the

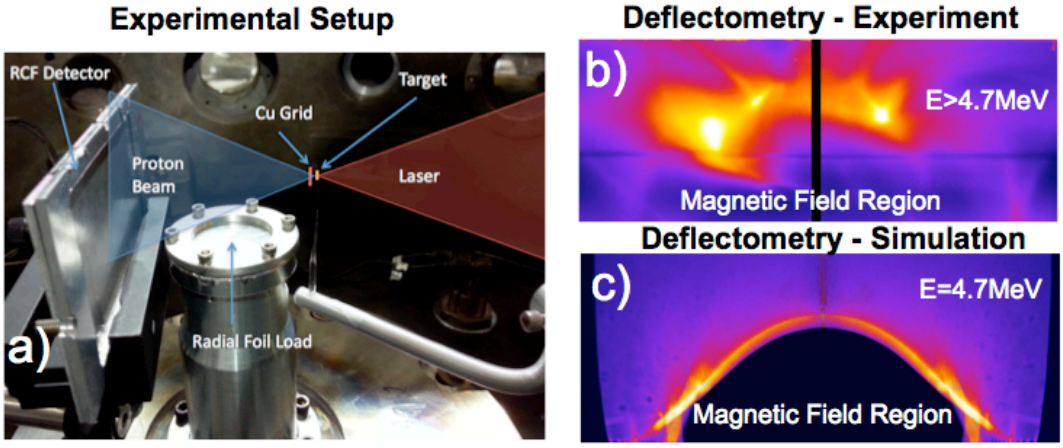

Fig. 10. (a) Picture of setup for proton probing of radial foil generated plasma. (b) RCF deflected protons at 250 ns after current start. Dome shape from protons which are deflected out of field carrying region. (c) Simulated RCF signal from Gorgon at the same time and location as the RCF above it.

central jet [17-20].

There was also potential proton flux loss due to collisional stopping within the plasma. The higher energy component of the proton spectrum has a sufficiently long mean free path that collisions can largely be neglected. With these systems, a significant amount of mass is ablated, which produces a long scale-length plasma which is capable of stopping the lowest energy component of the proton beam. For example, the energy loss in plasmas can be estimated using the following general formula [21-24].

$$-\frac{1}{Z_t^{\,2}}\frac{dE}{dx} = \left(\frac{\omega_p e}{v_t}\right)^2 \left[G\left(\frac{v_t^2}{v_{th}^2}\right) \ln\Lambda + H\left(\frac{v_t}{v_{th}}\right) \right]$$

Using appropriate values for the plasma of interest and an initial proton energy of 7 MeV, a conservative estimate of the energy loss is dE/dx ~ 0.5 MeV/cm. For the radial foils

systems, where the plasma scale length is ~ 1 cm, this corresponds to an overall energy loss of ~ 1 MeV. These losses are evident in the first layer of RCF, where the energy loss is greater, and the stopped energy due to filters was typically ~ 1.2 MeV. For the higher energy protons, corresponding to the deeper layers of RCF, stopping is much less of a concern since energy losses become significantly less than the energy windows for the RCF layers, however the contrast of the mesh imprinted on the beam was degraded significantly.

There is one apparent difference between the experiment and the simulations shown in Fig 10. This disparity is the appearance of the two divergence features near the top of the dome-like feature in the experimentally obtained images. These features, as in the short-circuit shots, are most likely an indication of the strength of the field produced by current flowing vertically. By measuring the separation between the two features, and the relative angle between them, an estimation of the amount of current flowing in the plasma can be made. Assuming that the diameter of the jet/current carrying region, a current of ~200 kA at 250 ns is calculated, which is in good agreement with the current measurements by the B-dots used in the Zebra chamber. Successive shots of the same type of load at various delays indicate the evolution of the system. Beyond this time, there is likely significantly more magnetic field entrained in the plasma load, as indicated by the deflection of protons out of a magnetic field region well after the current pulse is expected to have diminished. In later shots, the dome shape persists up to ~350 ns. This indicates that even without the presence of a driving current, magnetic field is still trapped in the so-called "magnetic bubble" as it travels away from its original position. This incongruity may be explained by a simplification applied in the simulations, where the Zebra current pulse is approximated as a $\sin^2$ waveform. This simplified current pulse returns to 0 at 400ns, whereas in the experiment the current was occasionally crow-barred at some time after peak current, >~300 ns, and the actual current delivered into the load after this point was unknown. It may also be due to the resistivity model used by Gorgon. This issue is presently under further investigation via more detailed modeling and analysis.

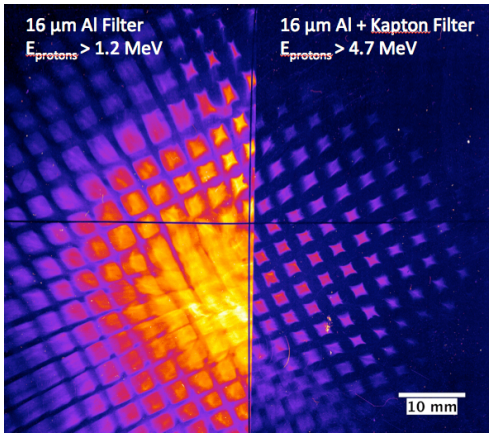

Fig. 11. Flux difference observed when two halves of RCF stack were covered with the two filter types during the same shot, with 127 µm Cu mesh in place.

In addition to the radial foil loads, several other load types were examined during a recent campaign. Among these loads were hybrid x-pinches and cylindrical wire arrays. The application of proton deflectometry to other types of plasma loads presents another challenge compared to short-circuit, radial foil, or radial wire arrays, which is the debris. Nearly all z-pinch loads will accelerate material to speeds on the order of ~10km/s. This is especially important in loads such as single wires, where the material is completely ballistic in areas where the magnetic field is unable to confine it, as well as in all other load types after the pinching force has diminished. To combat this issue, a blast shield was placed near the proton target in order to reduce the amount of debris reaching the OAP.

Additionally, the filtering used to wrap the RCF needed to be mechanically enhanced, so a layer of 35 um Kapton tape was placed in front of the Al foil. This, however, meant that our minimum detectable proton energy was significantly increased from ~1.2 MeV to ~4.7 MeV. The difference is illustrated in Figure 11. Here, the right side of the RCF was covered with the Al + Kapton tape filtering, while the left was Al foil only. It is apparent that some flux is lost due to the heavier filtering, which also affects the grid contrast at higher energies. Earlier tests confirmed that the damage to the RCF pack was too significant if the Kapton was not used. In order to boost the grid contrast at higher proton energies, thicker, 127 μm, Cu grids were employed. This is different than the previous experimental campaigns, where thin, 20 μm thickness, Cu grids were employed. PSTAR projected ranges predict that only protons with an energy greater than ~6.5 MeV will pass through the thicker 127 μm Cu grids, whereas the 20 μm grids will stop energies which are below ~ 2.1 MeV.

Hybrid x-pinches were first developed at Cornell University [25]. The setup is shown in part (a) of Fig 12. Two conical electrodes with a small hole drilled through the center are spaced ~ 600 um - 1mm apart, while a wire is threaded between them. Typically, such a setup is used to replicate an x-pinch, or micro-pinch, so that a single x-ray source can be used for radiography. The advantage over a standard x-pinch, is the ease with which they can be loaded, and the ease with which the mass at the "cross point" can be varied, which determines the timing of the pinch, and therefore the timing of the image. In this case, the load was chosen in order to create a small-scale plasma with a large-magnitude magnetic field, while drastically reducing the amount of debris ejected compared to a true x-pinch or single wire system. As in part (b) of Figure 12 proton radiograph was taken by firing Leopard only, without Zebra driving the load. This established the background image with which the ensuing data could be compared. The reduced contrast in the mesh image, due to the heavier filtering required for RCF survival during these shots, means that no clear grid remains in the data. There is still a significant amount of information in such a shot, however. Contrary to the short circuit case, the deflection features near the edges of the RCF, seen in Fig, 12 (c), are not the most relevant data. In this case, the feature, which is in the center of the image, contains the most interesting information. From this data, it is possible to estimate the field strength, width of the current-carrying region, and vertical extent of the plasma at the "cross point". Of course, the data near the edges does provide a general sanity check, as a global magnetic field magnitude check. By scanning parameter space with simulations, it will be

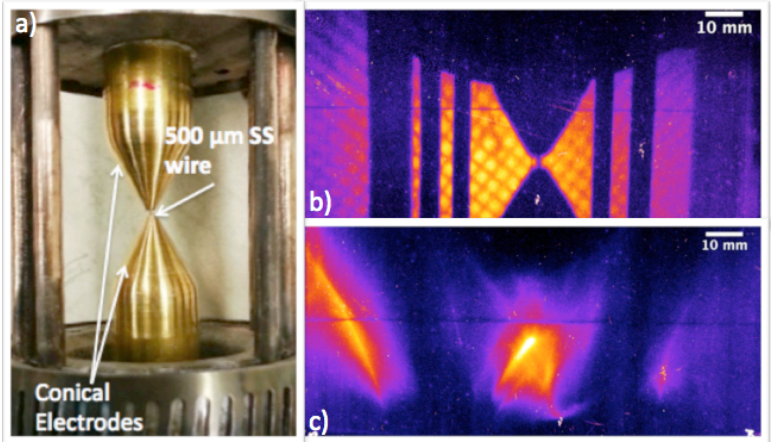

Fig. 12. (a) Picture of the experimental electrode load setup of a hybrid x-pinch. (b) Proton radiograph of the load & hardware. (c) Proton deflectogram taken near peak Zebra current.

possible to recover the details of this information. Initial simulations appear to disagree in magnitudes, although the general features are well reproduced. This incongruity could arise from the small differences between the simulated experimental hardware. In the experiment, the electrodes were designed such that one of the holes in the electrode tightly fit around the wire, so that the contact was assured, while the opposite hole was left slightly larger, in order to accommodate the loading procedure. This is of little concern for Zebra, since large ~ MV potentials will eventually ionize the wire and electrodes and fill this gap, however, the delay in this process could cause a difference in timing which would not be present in Gorgon.

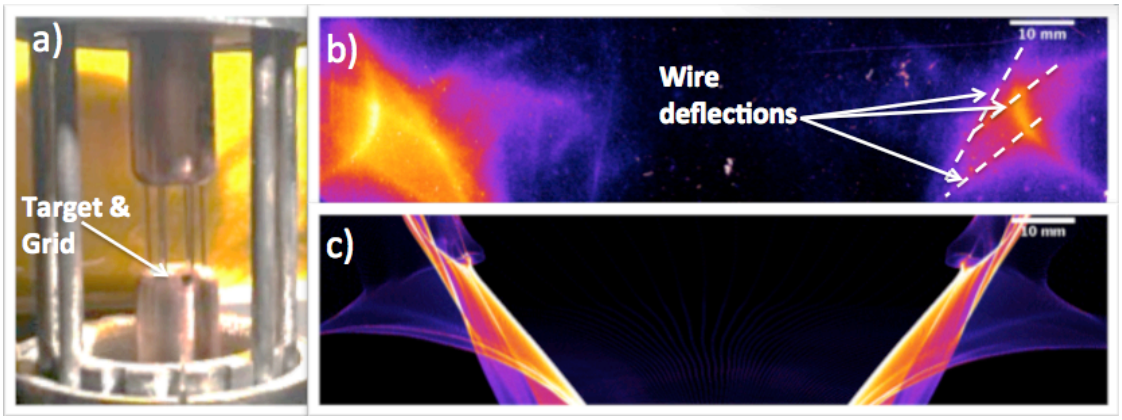

Fig. 13 (a) Picture of the cylindrical load, pre-shot. (b) Deflectogram of the cylindrical load taken near Zebra peak current with four primary features, per side, visible. (c) Simulated deflectogram of the cylindrical load from Gorgon at Zebra peak current.

The first application of proton deflectometry to cylindrical wire arrays was also carried out. Loads were comprised of 6 wires, 500 μm diameter stainless steel, placed at a 8 mm diameter, with an array height of ~ 10 mm. This load was not designed to implode, but rather as a magnetic field configuration test. The load is pictured in Figure 13 (a) just before a shot. Again, there is good agreement between experiment and simulation. A key difference, however, lies in the vertical extent of the experimental beam. Since, in this case, the Gorgon proton-probing post-processor is used to replicate results, the vertical extent is not truncated by the hardware as it is in the experiment. Again, the weak contrast of the grid means that there is little or no information provided by the mesh imprint. The prominent features are the four strongly visible streaks on each side of the image. These are deflection features similar to those in the short circuit case, and are due to the proton beam's encounter with the individual wires, as well as a fourth feature, which is related to the proton beam's response to the global magnetic field. Extensive simulation work is under way to reveal the detailed nature of the recently obtained results, and the implications they have concerning the physics of pulsed power driven plasma loads.

In this project two graduate students and two undergraduate students were trained; one at University of California San Diego and one at University of Nevada, Reno. The **broader impact** also included two undergraduate students, who were funded from this project and participated in experiments throughout the project duration. The graduate

students presented their work at the various domestic and international conferences. In addition, project findings were disseminated to high quality journals. A list of publications is given at the end of the report. The **intellectual merit** of the program was that it investigated strongly driven MHD systems and the influence of magnetic field topology on plasma evolution in pulsed power driven plasmas. The experimental program involved intense field-matter interaction in the generation of the proton probe, as well as the generation of plasma subjected to 1 MegaGauss scale magnetic fields. The computational aspect included two well-documented codes, in combination for the *first time* to provide accurate interpretation of the experimental results.

3. Summary

In summary, we have successfully demonstrated the first measurements of magnetic field produced by a pulsed power machine via proton deflectometry. We have modeled the dynamics of metal and plasma pulsed power loads. For basic loads, tracked particle patterns matched well to the experimental measurement, allowing quantitative fitting of the magnetic field strength and topology. From the short circuit data, simulation data can determine magnetic field magnitudes within ~15% of the calculated value. Data from a radial foil load illuminated a magnetic bubble structure at 10 snapshots throughout its evolution that agree with the expectation from modeling and also showed evidence of a high current jet. Several challenges were overcome to apply the method to complex plasma loads. Reliable data for such plasmas were taken, but further modeling and analysis are required for their interpretation. This detailed modeling and analysis is ongoing to facilitate the interpretation of the measurements which will enhance the understanding of the underlying physics of current flow and magnetic field generation in such complicated high energy density plasma systems driven by high current pulsed power drivers. Future work will examine the field configurations in other common z-pinch plasma loads, such as x-pinches, single wires, and planar wire arrays as part of the UCSD student's dissertation.

4. Refereed Journal Publications

1. "Measurement of Magnetic Field Configuration in Pulsed Power Driven Experiments via Proton Deflectometry"
   D. Mariscal, C. McGuffey, J. Valenzuela, M. S. Wei, F. N. Beg, R. Presura, and J. P. Chittenden,
   Applied Physics Letters, to be submitted (October, 2013).

2. "Study of X-pinch dynamics using a low current (25 kA) and slower current (400 ns) pulse"
   G. W. Collins IV, M. P. Valdivia, T. Zick, R. E. Madden, M. G. Haines, and F. N. Beg,
   Phys. Plasmas **20**, 042704 (2013)

3. "Plasma Pinch Research on University Pulsed-Power Generators in the United States"

J. L. Giuliani, F. N. Beg, R. M. Gilgenbach, V. L. Kantsyrev, B. R. Kusse, V. V. Ivanov, and R. Presura
IEEE Transactions on Plasma Science **40**, 3246 - 3264 (2012).

4. "Mapping return currents in laser-generated Z-pinch plasmas using proton deflectometry"
M. J.-E. Manuel, N. Sinenian, F. H. Séguin, C. K. Li, J. A. Frenje, H.G. Rinderknecht, D. T. Casey, A. B. Zylstra, R. D. Petrasso, and F. N. Beg,
Applied Physics Letters **100**, 203505 (2012).

5. "Experimental Analysis of the Acceleration Region in Tungsten Wire Arrays,"
S. C. Bott, D. Mariscal, K. Gunasekera, J. Peebles, F. N. Beg, D. A. Hammer, B. R. Kusse, J. B. Greenly, T. A. Shelkovenko, S. A. Pikuz, I. C. Blesener, R. D. McBride, J. D. Douglass, K. S. Blesener, and P. F. Knapp,
IEEE Transactions on Plasma Science **40**, 3324-3328 (2012).

6. "A collinear self-emission and laser-backlighting imaging diagnostic"
S. C. Bott, G. Collins, K. Gunasekera, D. Mariscal, F. N. Beg, D. M Haas, F. Veloso, I. C. Blesener, A. D. Cahill, C. L. Hoyt, B. R. Kusse, and D. A. Hammer,
Review of Scientific Instruments **83**, 083507 (2012).

7. "Effect of the global to local magnetic field ratio on the ablation modulations on X-pinches driven by 80 kA peak current"
G. W. Collins IV, D. Marsical, D. M. Haas, R. E. Madden, K. Gunasekara, J. Kim, M. L. L. Abarr, S. C. Bott, J. P. Chittenden, F. N. Beg
New Journal of Physics **14** 043021(2012).

8. "Examination of Bow-Shock Formation in Supersonic Radiatively Cooled Plasma Flows"
J. L. Peebles, S. C. Bott, K. Gunasekera, K. Joohwan, L.Harpster, B. Evans, D. Gomez, O. Paran, C. Peterson, and F. N. Beg,
IEEE Transactions on Plasma Science **39**, 2422,2423, (2011).

9. "250 kA Compact Linear Transformer Driver for Wire Array Z-Pinch Loads"
S. C. Bott, D. M. Haas, R. E. Madden, U. Ueda, Y. Eshaq, G. Collins IV, K. Gunasekera, D. Mariscal, J. Peebles, F. N. Beg, M. Mazarakis, K. Struve, and R. Sharpe,
Physical Review **14** (special issue on accelerators and beams), 050401 (2011).

10. "Supersonic Jet Formation and Propagation in X-Pinches"
D. M. Haas, S. C. Bott, J. Kim, D. A. Mariscal, R. E. Madden, Y. Eshaq, U. Ueda, G. Collins IV, K. Gunasekera, F. N. Beg, J. P. Chittenden, N. Niasse and C. A. Jennings," Supersonic Jet Formation and Propopagation in X-Pinches," *Astrophys. Space Sci*. DOI 10.1007/s10509-011-0599-8 (2011).

11. "Ablation Studies of Low-Number Wire Arrays at 200 kA Using A Linear Transformer Driver"
S. C. Bott, D. M. Haas, Y. Eshaq, Utako Ueda, Robert E. Madden, Gilbert W. Collins IV, and Farhat N. Beg,
IEEE Transactions on Plasma Science **38**, 567 (2010).

12. "Effect of current rise-time on the formation of the precursor column in cylindrical wire array z-pinches at 1 MA"
S. C. Bott, D. M. Haas, Y. Eshaq, U. Ueda, F. N. Beg, D. A. Hammer, B. Kusse, J. Greenly, T. A. Shelkovenko, S. A. Pikuz, I. C. Blesener, R. D. McBride, J. D. Douglass, K. Bell, P. Knapp, J. P. Chittenden, S. V. Lebedev, S. N. Bland, G. N. Hall, F. A. Suzuki-Vidal, A. Marocchino, A. Harvey-Thomson, J. B. A. Palmer, A. Esaulov, D. J. Ampleford, M. G. Haines,
Phys Plas. **16**, 072701 (2009).

13. "Investigation of Carbon X-pinches as a Source for Point Projection Radiography"
R. E. Madden, S. C. Bott, G. Collins and F. N. Beg,
IEEE Transactions on Plasma Science **37**, 433 (2009).

References

[1] M. Borghesi *et al*., Phys. Plasmas **9**, 2214 (2002)

[2] A.J. Mackinnon *et al*., Rev. Sci. Instrum. **75**, 3531 (2004).

[3] M. Borghesi *et al*., Rev. Sci. Instrumen.**74**, 1688 (2003).

[4] M. Borghesi *et al*., Laser Part. Beams **25**, 161 (2007).

[5] M. Borghesi et al., Laser Part. Beams **23**, 291 (2005).

[6] L. Romagnani *et al*., Laser Part. Beams **26**, 241 (2008).

[7] M. Key *et al*., *Journal of Fusion Energy* **17**, p231, (1998).

[8] F. N. Beg et al., *Plasma Phys. Controlled Fusion* **1**, 1 (1997).

[9] S.C. Wilks *et al*., Physics of Plasmas **8**, 542 (2001).

[10] C.K. Li *et al*., Rev. Sci. Instrum.**77**, 10E725 (2006).

[11] C. K. Li *et al*., Phys. Rev Lett. **97**, 135003 (2006).

[12] C. K. Li *et al*., Phys. Rev Lett. **99**, 015001 (2007).

[13] C. K. Li *et al*., Phys. Rev Lett. **100**, 225001 (2008).

[14] see for example http://www.srim.org/

[15] S V Lebedev *et al*., Plasma Phys. Control. Fusion **47**, B465 (2005).

[16] J.P. Chittenden *et al*., *Plasma Phys. Control. Fusion* **46**, pB457 (2004).

[17] D. R. Welch *et al*., *Nucl. Instrum. Methods Phys. Res. A* **464**, 134, (2001).

[18] A. Ciardi *et al*., Astrophys. J. Lett. **691**, L147 (2009).

[19] F. Suzuki-Vidal et al., Astrophys. Space Sci. **322**, 19 (2009).

[20] P. Gourdain *et al*., Phys. Plasmas **17**, 012706 (2010).

[21] D.G. Hicks *et al*., Phys. Plasmas **7**, p5106 (2000).

[22] T. A. Mehlhorn, J. Appl. Phys. **52**, 6522 (1981).

[23] T. Peter, and J. Meyer-ter-Vehn, Phys. Rev. A **43**, 1998 (1991).

[24] C. K. Li, and R. D. Petrasso, Phys. Rev. Lett. **70**, 3059 (1993).

[25] T. A. Shelkovenko, *et al*., Phys. Plasmas **17**, 112707 (2010).